Signatures of Environment-Induced Quantum Synchronization Transitions via Two-body Dissipator Engineering

Xingli Li[1], Yan Li[1], and Yangqian Yan[1,2,3*]

[1]*Department of Physics, The Chinese University of Hong Kong, Shatin, New Territories, Hong Kong, China*
[2]*State Key Laboratory of Quantum Information Technologies and Materials, The Chinese University of Hong Kong, Hong Kong SAR, China*
[3]*The Chinese University of Hong Kong Shenzhen Research Institute, Shenzhen 518057, China*

(Received 2 November 2025; accepted manuscript online 31 December 2025)

Metronome synchronization and the transition between the in-phase and anti-phase synchronization have been observed in classical systems. We demonstrate the quantum analog of this phenomenon in a two-qubit system coupled to a common environment. Tracing out the environment in the quantum collision model, we obtain an effective master equation with a two-body dissipator for two qubits. Quenching the two-body dissipator, we demonstrate controlled transitions from in-phase to anti-phase synchronization. This synchronization transition is robust against noise. Signatures of the transition are observed through Pearson correlation coefficient measurements obtained via quantum simulations on superconducting circuits. Future experiments employing qutrit systems are expected to yield a more pronounced effect.

DOI: 10.1088/0256-307X/43/2/020302 CSTR: 32039.14.0256-307X.43.2.020302

1. Introduction. In-phase and anti-phase synchronization have been observed in classical metronome systems placed on movable platforms. It has also been demonstrated that the transition between these synchronization states can be achieved by engineering the common environment [Fig. 1(a)], i.e., by tuning the properties of the shared platform.[1,2] To date, research on synchronization has expanded into the quantum domain, with numerous studies exploring synchronization in a wide range of open quantum systems,[3–17] like van der Pol oscillators[18–20] and spin chains.[21–23] Synchronization has also been demonstrated across diverse platforms such as cold atoms,[24] trapped ions,[25,26] nuclear spins,[27] and superconducting circuits.[28]

While the classical synchronization transitions can be induced purely by modifying the common environment without altering the coupling form between the metronomes and the movable platform, the quantum version of transitions between in-phase and anti-phase synchronization typically relies on adjusting the inter-system couplings.[29,30] This highlights a fundamental gap: a quantum framework for environmental engineering, in which dissipation is tuned to control synchronization, remains underdeveloped. To bridge this gap, we introduce a pathway for dissipation engineering: controlling the dissipation by designing the states of the environment, while leaving the system-environment interaction Hamiltonian unchanged.

To achieve it in a quantum system, we utilize the quantum collision model (QCM),[31–41] which is also known as the repeated-interaction scheme [Fig. 1(b), see Supplementary Materials (SM) for details].[42–48] The QCM provides a versatile platform for engineering the environment, as it allows for precise control over the states of individual ancillas and their interactions with the system. Furthermore, since the interaction between the ancillas and system is unitary, it can be easily realized on quantum circuits.[39] Within our model, we introduce a "quantum analog" of the classical metronome synchronization experiment: two noninteracting qubits ("quantum metronomes") couple to the common environment ("movable platform"), which may lead to dissipative coupling, as shown in Fig. 1(a). We have the following findings: (i) Synchronization, which is robust to noise, spontaneously emerges in quantum systems once a weak coupling is established through a common environment. (ii) Tracing out the environment, we obtain an effective master equation with its two-body dissipator determined by the state of the environment. While one-body dissipator and dark state engineering have been extensively studied,[49–52] to the best of our knowledge, two-body dissipator engineering has not been previously well explored. (iii) We demonstrate the transition of in-phase and anti-phase synchronization via quenching the environment, or effectively, the two-body dissipator. (iv) We observe the signatures of the transition from the Pearson correlation coefficient by performing quantum simulation on superconducting qubits.

2. Model. The Hamiltonian of "metronomes" reads $H_{\rm S} = \sum_{j=1,2} \hbar\omega\sigma_j^z$, where σ_j^z is the Pauli matrix and ω is half the transition frequency. We model the environment as a stream of three-level ancillas (qutrit), labeled as $\{|g\rangle, |e\rangle, |r\rangle\}$. Each ancilla sequentially interacts

*Corresponding author. Email: yqyan@cuhk.edu.hk
© 2026 Chinese Physical Society and IOP Publishing Ltd. All rights, including for text and data mining, AI training, and similar technologies, are reserved.

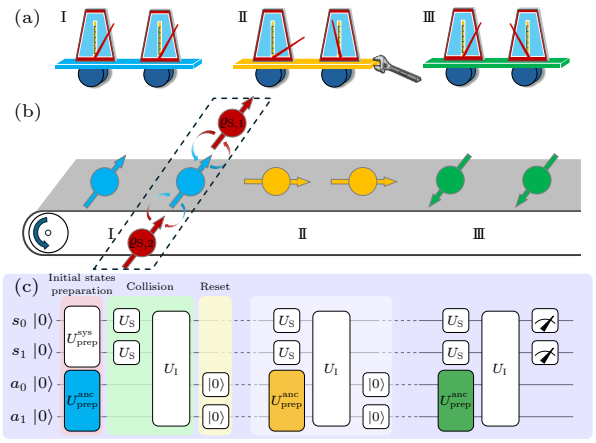

Fig. 1. (a) Schematics of classical synchronization transition with two metronomes coupled by a common movable platform. The transition from in-phase (I) to anti-phase (III) synchronization can be realized by tuning the movable platform (II). (b) Schematics of the QCM. The two qubits $\varrho_{S,1(2)}$ interact stroboscopically with ancilla qutrits (environment). Different ancilla states lead to different effective dissipators for the qubits. Quantum synchronization transition is induced by quenching the ancilla state. (c) Schematics of the quantum circuit that simulates the QCM.

with "metronomes" [Fig. 1(b)], governed by the interaction Hamiltonian: $H_I = \hbar g(\sigma_1^- \otimes |r\rangle\langle g| + \sigma_2^- \otimes |r\rangle\langle e| + \text{H.c.})$, where g is the coupling strength, σ_j^- is the lowering operator for the j-th qubit. The evolution operator U during a collision period, consists of two contributions: $U = U_I U_S = e^{-iH_I\tau/\hbar}e^{-iH_S\tau/\hbar}$, where τ is the time for each collision. After interacting with the ancilla state η_E^{n+1} at the $(n+1)$-th collision, the density matrix of the system ϱ_S^n evolve according to a quantum map Φ,

$$\varrho_S^{n+1} = \Phi[\varrho_S^n] := \text{tr}_{\eta_E^{n+1}}[U\varrho_S^n \otimes \eta_E^{n+1}U^\dagger]. \quad (1)$$

Altering ancilla states enables us to engineer the properties of the environment or the quantum analog of "movable platform". Under Markov approximation, we obtain that, for any given ancilla state $\eta_E = |\psi_E\rangle\langle\psi_E|$, where $|\psi_E\rangle = \cos\theta|g\rangle + \sin\theta e^{i\phi}|e\rangle$, QCM predicts the effective master equation (see SM for detailed derivation) as

$$\frac{d}{dt}\varrho_S = -\frac{i}{\hbar}[H_S, \varrho_S] + \frac{g^2\tau}{\hbar^2}\mathcal{D}_{\varrho_S}[\cos\theta\sigma_1^- + \sin\theta e^{i\phi}\sigma_2^-], \quad (2)$$

where $\mathcal{D}_{\varrho_S}[o] = o\varrho_S o^\dagger - \frac{1}{2}(o^\dagger o\varrho_S + \varrho_S o^\dagger o)$ is the effective dissipator. We consider three distinct dynamical phases: for $|\psi_E\rangle_I$ in **Phase I**, $\theta = \pi/4$, $\phi = \pi$; for $|\psi_E\rangle_{II}$ in **Phase II**, $\theta = 0$; and for $|\psi_E\rangle_{III}$ in **Phase III**, $\theta = \pi/4$, $\phi = 0$. The above master equation can be viewed as the system interacting with a bath of multiple ancillas,[53] or as the system interacting with an ancilla, yet the ancilla itself is undergoing significant spontaneous emission (see SM).

Before we discuss the synchronization transition, we explain the synchronization mechanism within our system through Eq. (2): two-body dissipation gives rise to dark states and decoherence-free subspace spanned by dark states.[18] A dark state $|\psi_{D,j}\rangle$ is defined as a state that is immune to dissipative process, i.e., $o|\psi_{D,j}\rangle = 0$, with $H_S|\psi_{D,j}\rangle = \epsilon_j|\psi_{D,j}\rangle$. Thus, the corresponding eigenoperators $A_{jk} = |\psi_{D,j}\rangle\langle\psi_{D,k}|$ satisfy $\mathcal{D}_{A_{jk}}[o] = 0$. For instance, in the case of $\mathcal{D}_{\varrho_S}[(\sigma_1^- - \sigma_2^-)/\sqrt{2}]$, which corresponds to Phase I, two dark states emerge: the ground state $|\psi_{D,1}\rangle = |\downarrow\downarrow\rangle$ and the symmetric state $|\psi_{D,2}\rangle = (|\downarrow\uparrow\rangle + |\uparrow\downarrow\rangle)/\sqrt{2}$, where $|\downarrow\rangle$ and $|\uparrow\rangle$ denote the eigenstates of σ^z. In the long-time limit, the steady-state density matrix reads $\varrho_S^{ss} \sim \sum_{j,k=1,2} c_{jk}e^{i(\varepsilon_k - \varepsilon_j)n\tau}A_{jk}$, the constants c_{jk} are determined by the initial state, satisfying $c_{11} + 2c_{22} = 1$ to preserve trace. In this study, we employ the x-direction magnetizations as the order parameter, denoted by $\langle\sigma_j^x\rangle_n = \text{tr}[\varrho_S^n\sigma_j^x]$, to signify the phase relationship between the two spins. Note that when c_{11} or c_{22} equals 0, the final density matrix is a pure state and there exists no oscillation in the order parameter; for a pure state, the oscillation reaches its maximum at $c_{11}/c_{22} = 2$. Likewise, for $\mathcal{D}_{\varrho_S}[\sigma_1^-]$, dark states are $|\psi_{D,1}\rangle = |\downarrow\downarrow\rangle$ and $|\psi'_{D,2}\rangle = |\downarrow\uparrow\rangle$, and for $\mathcal{D}_{\varrho_S}[(\sigma_1^- + \sigma_2^-)/\sqrt{2}]$, dark states are the ground state $|\psi_{D,1}\rangle = |\downarrow\downarrow\rangle$ and the antisymmetric state $|\psi''_{D,2}\rangle = \frac{|\downarrow\uparrow\rangle - |\uparrow\downarrow\rangle}{\sqrt{2}}$. Through the decomposition of steady state, we reexpressed the order parameters as $\langle\sigma_j^x\rangle \sim \text{tr}[(A_{12} + A_{21})\sigma_j^x]$. Therefore, the phase difference between them is determined by the dark states, i.e., in-phase in the presence of $|\psi_{D,2}\rangle$, anti-phase in the presence of $|\psi''_{D,2}\rangle$.

3. Synchronization Transitions. With the knowledge of correspondence between the targeting dissipator and the state of environment (ancilla), we now proceed to demonstrate the synchronization transition. We initialize "quantum metronomes" in a random separable state, and prepare the ancilla in Phase I: $|\psi_E\rangle_I$, steering the "metronomes" towards achieving in-phase synchronization.

The solid and dashed lines in Fig. 2(a) show the evolution of order parameters $\langle\sigma_1^x\rangle$ and $\langle\sigma_2^x\rangle$, respectively. The system transits from initial asynchronous behavior ($n \lesssim 700$) to synchronization, which is consistent with our theoretical prediction. To transit to the anti-phase synchronization, the final ancilla state has to be $|\psi_E\rangle_{III}$. However, the projection from the final state of the in-phase synchronization phase to the decoherence-free subspace of the anti-phase synchronization results in state $|\psi_{D,1}\rangle$ only. As we argued earlier, a single dark state cannot induce oscillation in the order parameters. To circumvent this issue, we introduce an intermediate transition phase Phase II, where the ancilla state is $|\psi_E\rangle_{II} = |g\rangle$. The dark state of this phase has finite overlap with both $|\psi_{D,2}\rangle$ and $|\psi''_{D,2}\rangle$, thus making the transition from in-phase to anti-phase synchronization possible. As shown in Fig. 2(a), we quench the ancillas into Phase II after $n = 1600$ with $|\psi_E\rangle_{II} = |g\rangle$, and further quench the ancilla states to Phase III at $n = 1720$ to drive the system from in-phase synchronization to anti-phase synchronization.

To quantitatively assess the synchronization transition, we calculate the Pearson correlation coefficient C_{x_1,x_2} between the two order parameters as a function of n,[54–56]

$$C_{\alpha,\beta}(n) = \frac{\sum_{j=n}^{n+\Delta n}(\alpha_j - \bar{\alpha})(\beta_j - \bar{\beta})}{\sqrt{\sum_{j=n}^{n+\Delta n}(\alpha_j - \bar{\alpha})^2 \sum_{j=n}^{n+\Delta n}(\beta_j - \bar{\beta})^2}}, \quad (3)$$

i.e., the ratio of the covariance to the respective standard deviations of discrete-time series data; here $\bar{\alpha} = \Delta n^{-1}\sum_{j=n}^{n+\Delta n}\alpha_j$ and $\bar{\beta} = \Delta n^{-1}\sum_{j=n}^{n+\Delta n}\beta_j$ denote the temporal averages, where Δn is the sample length of the discrete data. The green dashed line in Fig. 2(a) illustrates the progression of the Pearson correlation from initial unstable values to 1 (in-phase synchronization) and eventually to -1 (anti-phase synchronization).

The establishment of quantum synchronization typically involves entanglement generation. To quantify entanglement, we adopt one of the popular choice for two-level systems, the concurrence[57] $\mathcal{C}(\varrho_{\rm S}^n) \equiv \max(0, \sqrt{\lambda_1} - \sqrt{\lambda_2} - \sqrt{\lambda_3} - \sqrt{\lambda_4})$, where λ_j is the eigenvalue of $\varrho_{\rm S}^n\tilde{\varrho}_{\rm S}^n$ in decreasing order, and $\tilde{\varrho}_{\rm S}^n$ is the spin-flipped state, defined as $\tilde{\varrho}_{\rm S}^n = (\sigma_y\otimes\sigma_y)\varrho_{\rm S}^{n*}(\sigma_y\otimes\sigma_y)$, where $\varrho_{\rm S}^{n*}$ is the complex conjugate of $\varrho_{\rm S}^n$ and σ^y is the Pauli matrix. Concurrence takes values in the range $[0,1]$, where 0 indicates a separable state and 1 represents a maximally entangled state. Concurrence is defined for both pure and mixed states and is non-increasing under local operations and classical communication,[58] making it one of the ideal quantifiers of entanglement in two-qubit systems. Meanwhile, correlations are assessed using the mutual information $I(\varrho_{\rm S}^n) \equiv S(\varrho_{{\rm S},1}^n) + S(\varrho_{{\rm S},2}^n) - S(\varrho_{\rm S}^n)$, where $S(\cdot)$ is the von Neumann entropy and $\varrho_{{\rm S},j}^n = {\rm tr}_{k,k\neq j}[\varrho_{\rm S}^n]$ is the reduced density matrix.

The squares and circles in Fig. 2(b) show the concurrence and mutual information, respectively, as a function of the number of collisions n. In Phase I, mutual information emerges rapidly and reaches a plateau, while entanglement generation lags. This is due to the fact that concurrence is a measure of quantum correlations, while mutual information encompasses both classical and quantum correlations. That is, classical correlations develop first. As entanglement increases, synchronization gradually establishes, which further boosts the rise of mutual information again until both reach a plateau. In Phase Ⅱ, the ancilla quenching decouples the "metronomes", causing both measures to decay. In Phase Ⅲ, both correlations continue to decline, eventually vanish, and then revive.

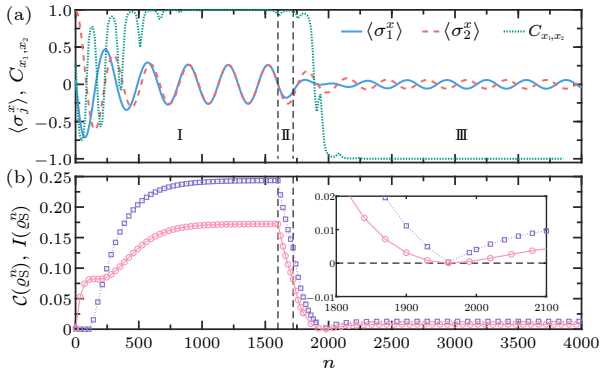

Fig. 2. (a) The blue solid, red dashed, and green dotted lines show the order parameter $\langle\sigma_1^x\rangle$, $\langle\sigma_2^x\rangle$, and their Pearson correlation C_{x_1,x_2} as a function of the collision number n, respectively. As n increases, ancilla state changes from $|\psi_{\rm E}\rangle_{\rm I}$ (Phase I) to $|\psi_{\rm E}\rangle_{\rm II}$ (Phase Ⅱ) and $|\psi_{\rm E}\rangle_{\rm III}$ (Phase Ⅲ). (b) The circles and squares show mutual information $I(\varrho_{\rm S}^n)$ and entanglement $\mathcal{C}(\varrho_{\rm S}^n)$ as a function of n, respectively. The inset shows the zoom-in where mutual information and entanglement reach zero. Here $\omega\tau = 0.01$, $g^2\tau = 1$, sample length $\Delta n = 140$, and the randomly selected initial state is $|\psi\rangle_{\rm S}^{\rm ini} = [0.8579 + 0.2631{\rm i}, 0.2774 + 0.3013{\rm i}, 0.0222 - 0.1480{\rm i}, 0.0428 - 0.0532{\rm i}]^{\rm T}$ with T denotes the transpose.

We now explain the mechanism for the delayed vanishing and revival of the entanglement by a three-level system. Due to the absence of coherent pumping in Eq. (2), the system can be simplified by adiabatically eliminating the rapidly decaying excited state $|\uparrow\uparrow\rangle$. The resulting Hilbert space is exactly the union of all the decoherence-free subspaces at different phases. Within this subspace, the concurrence of the system is analytically tractable: $\mathcal{C}(\varrho_{\rm S}) = |c_0{\rm tr}[|\downarrow\uparrow\rangle\langle\uparrow\downarrow|\varrho_{\rm S}]|$, where $|\cdot|$ denotes absolute value and c_0 is the proportionality constant (see SM). The revival stems from sign changes in c_0 during in-phase/anti-phase transitions, as the population shifts from the symmetric to antisymmetric state, resulting in temporary nullification of entanglement.

4. Robustness to Noise. To test the noise robustness, we introduce an additional stochastic term $H_{\rm noise} = \sum_{j=1,2}\hbar\xi_j^\alpha(n)\sigma_j^\alpha$, where $\xi_j^\alpha(n)$ $(\alpha = x, y)$ represents random fluctuations within $[-\bar{\xi}, \bar{\xi}]$ at collision number n, where $\bar{\xi}$ controls the strength.

For controlled comparison across noise strength, we initialize the system to $|\psi\rangle_{\rm S}^{\rm ini} = (|\uparrow\uparrow\rangle + |\downarrow\uparrow\rangle)/\sqrt{2}$, purposely avoiding initial in-phase dynamics. Interestingly, since the noise could induce spontaneous departure from the decoherence-free subspace, Phase Ⅱ is redundant for synchronization transitions. To double check, we compare the complete sequence (Phase I→Ⅱ→Ⅲ) [Fig. 3(a)] with the sequence without Phase Ⅱ, i.e., (Phase I→Ⅲ) [Fig. 3(b)].

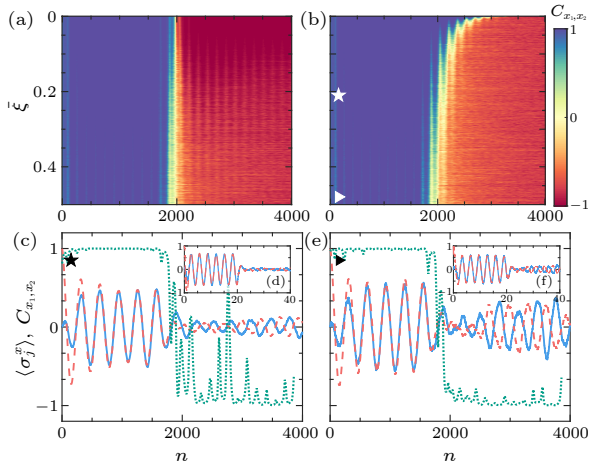

Fig. 3. Comparison of two ancilla quench sequences under noise. (a) and (b) For the complete sequence (Phase I →Ⅱ→Ⅲ) and the sequence without Phase Ⅱ, respectively. Both panels display Pearson correlation C_{x_1,x_2} as a function of collision number n and noise strength $\bar{\xi}$ with sample length $\Delta n = 140$. The blue solid, red dashed, and green dotted lines in panels (b) and (e) show $\langle\sigma_1^x\rangle$, $\langle\sigma_2^x\rangle$, and C_{x_1,x_2} as a function of the collision number n for $\bar{\xi} = 0.21$ and $\bar{\xi} = 0.49$, respectively, in the sequence without Phase II. The blue solid and red dashed lines in insets (d) and (f) show $\langle\sigma_1^x\rangle_{\rm traj}$ and $\langle\sigma_2^x\rangle_{\rm traj}$ along a single quantum trajectory, obtained from stochastic Schrödinger equation. The other parameters are the same as those in Fig. 2.

Figures 3(a) and 3(b) show the density plot of the Pearson correlation as a function of collision number n and noise strength $\bar{\xi}$. The transition is always clear regardless of noise strength, except that small enough noise leads to a delay in the transition for the sequence without Phase Ⅱ [see Fig. 3(b)]. In the zero-noise limit, the transition occurs at $n = \infty$, which is consistent with the theoretical prediction.

We illustrate the evolution of order parameters and Pearson correlation for the sequence without Phase Ⅱ under weak ($\bar{\xi} = 0.21$) and strong ($\bar{\xi} = 0.49$) noise in Figs. 3(c) and 3(e), respectively. The enhanced Pearson correlation with strong noise indicates that noise does help with the anti-phase transition. Notably, this robustness persists not only in ensemble averages but also at the single-trajectory level, as calculated via the stochastic Schrödinger equation[22,59–61] [Figs. 3(d) and 3(f), as well as SM]. The elimination of Phase Ⅱ is favored since it reduces the total time needed for a quantum simulation [see SM for discussion of the complete sequence].

5. Experimental Realization. We now turn to the experimental realization of our model on quantum circuits made of qubits. While the systems are made of two qubits, the ancilla states which consist of three energy levels need two qubits to encode. Thus, we need to first map our system-ancilla interaction model onto a quantum circuit model by encoding the ancilla states as $|g\rangle \mapsto |{\downarrow\downarrow}\rangle_{\rm QC}$, $|e\rangle \mapsto |{\downarrow\uparrow}\rangle_{\rm QC}$, and $|r\rangle \mapsto |{\uparrow\downarrow}\rangle_{\rm QC}$. The ancilla states are reset to the initial state after each collision with the two spins. We show the quantum circuit for our QCM in Fig. 1(c). Our QCM minimally requires four logical qubits: system qubits s_0, s_1 and ancilla qubits a_0, a_1, with a connectivity topology of s_0—a_0—a_1—s_1. We realize the simultaneous system-ancilla interactions via the second order Suzuki–Trotter decomposition[62] (see SM for detailed implementation).

The lines and squares in Fig. 4(a) shows the order parameters $\langle\sigma_j^x\rangle$ as a function of n for the QCM and ideal quantum circuits.[63] The excellent agreement validates the effectiveness of our mapping scheme. However, the cumulative errors from hardware noise and decoherence increase exponentially with the circuit depth, which is proportional to collision number n. To mitigate, we accelerate the system evolution such that $n \leq 12$ by setting $\omega\tau = 0.8$ and $g^2\tau = 4$, utilize the quench sequence without intermediate Phase II and triggering ancilla quench at $n = 5$, and initialize the system in a nearly in-phase synchronized state.

The circles with error bars in Figs. 4(b) and 4(c) show the order parameters $\langle\sigma_j^x\rangle$ as a function of n for the quantum simulation on the superconducting circuits (see detailed implementation in SM). Due to the destructive nature of quantum measurements, for each n, the experimental sequence starts from the initial state. To ensure statistical significance, for each data point, we repeat the measurement 25 times, each comprising 5000 shots of quantum circuit executions. We observe that the oscillation amplitude decays rapidly at first but stabilizes within a narrow range. Although the noise significantly

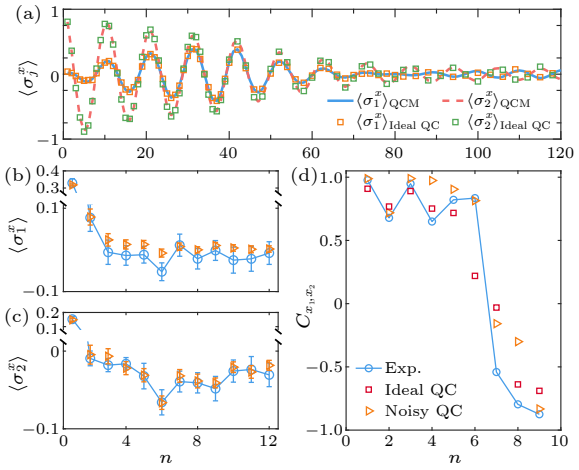

Fig. 4. (a) The lines and squares show $\langle\sigma_j^x\rangle$ as a function of collision number n for the QCM and ideal quantum circuits calculation (denoted by Ideal QC), respectively, with $\omega\tau = 0.3$ and $g^2\tau = 1$. (b) and (c) The circles and triangles with error bar show $\langle\sigma_j^x\rangle$ as a function of n computed via superconducting circuit simulation and noisy quantum circuits calculation, respectively, with $\omega\tau = 0.8$ and $g^2\tau = 4$. (d) The blue circles, red squares, and yellow triangles show the Pearson correlation C_{x_1,x_2} as a function of n computed via superconducting circuit simulation (Exp.), Ideal QC, and noisy quantum circuits calculation (Noisy QC), respectively, with a sample length $\Delta n = 4$.

affects the oscillation amplitude, we still observe weak in-phase ($n < 6$) and anti-phase ($n > 6$) oscillations. This is clearly shown by the Pearson correlation C_{x_1,x_2} [circles in Fig. 4(d)]. Our experimental results are largely consistent with noisy quantum circuit simulations (triangles in Fig. 4), which mimic realistic conditions by applying various noise channels, such as depolarizing or relaxation errors, to each gate operation. We expect that future simulations on quantum computers with a more suitable topology, such as qutrit-based circuits[64–67] could potentially yield improved results.

6. Conclusions. In summary, we have established a quantum analog of classical synchronization transition by engineering the state of ancilla, i.e., the environment of two noninteracting qubits. We have shown that the two-body dissipator can be engineered by quenching ancilla states, which leads to a transition from in-phase to anti-phase synchronization. This transition is robust against noise, and we have observed the signatures of synchronization transition from the Pearson correlation in quantum circuits simulations. Note that here, since the qubit does not exhibit nonlinearity, there exists no limit cycle. We expect the synchronization transition to be more stable for nonlinear systems with limit cycles, such as Van der Pol oscillators.[18]

Meanwhile, it is interesting to note that, by engineering the state of the ancilla, we obtain an effective master equation with a two-body dissipator with desired phase factors. Starting from a product state, we can eventually obtain a two-qubit entangled state through the dissipative coupling. We have also observed the vanishing and revival of entanglement and established the connec-

tion between entanglement behavior and synchronization transition. This is a step towards many-body dissipator engineering,[68] which is promising in realizing full control of many-body entangled states.

Acknowledgements. This work was supported by the Quantum Science and Technology-National Science and Technology Major Project (Grant No. 2024ZD0300600), the National Natural Science Foundation of China (Grant Nos. 92565105 and 12204395), Hong Kong RGC (Grant Nos. 14301425, 24308323, and C4050-23GF), Guangdong Provincial Quantum Science Strategic Initiative (Nos. GDZX2404004 and GDZX2505005), the Space Application System of China Manned Space Program, and CUHK Direct Grant.

References

[1] Kapitaniak M, Czolczynski K, Perlikowski P, Stefanski A, and Kapitaniak T 2012 *Phys. Rep.* **517** 1
[2] Kapitaniak M, Czolczynski K, Perlikowski P, Stefanski A, and Kapitaniak T 2014 *Phys. Rep.* **541** 1
[3] Mari A, Farace A, Didier N, Giovannetti V, and Fazio R 2013 *Phys. Rev. Lett.* **111** 103605
[4] Giorgi G L, Plastina F, Francica G, and Zambrini R 2013 *Phys. Rev. A* **88** 042115
[5] Bellomo B, Giorgi G L, Palma G M, and Zambrini R 2017 *Phys. Rev. A* **95** 043807
[6] Buča B, Tindall J, and Jaksch D 2019 *Nat. Commun.* **10** 1730
[7] Buča B, Booker C, and Jaksch D 2022 *SciPost Phys.* **12** 097
[8] Li W, Cheng J, Gong W J, and Li J 2023 *Phys. Rev. A* **108** 033518
[9] Nadolny T and Bruder C 2023 *Phys. Rev. Lett.* **131** 190402
[10] Vaidya G M, Mamgain A, Hawaldar S, Hahn W, Kaubruegger R, Suri B, and Shankar A 2024 *Phys. Rev. A* **109** 033718
[11] Solanki P, Krishna M, Hajdušek M, Bruder C, and Vinjanampathy S 2024 *Phys. Rev. Lett.* **133** 260403
[12] Cabot A, Giorgi G L, Galve F, and Zambrini R 2019 *Phys. Rev. Lett.* **123** 023604
[13] Shen Y, Mok W K, Noh C, Liu A Q, Kwek L C, Fan W, and Chia A 2023 *Phys. Rev. A* **107** 053713
[14] Wächtler C W and Platero G 2023 *Phys. Rev. Res.* **5** 023021
[15] Murtadho T, Vinjanampathy S, and Thingna J 2023 *Phys. Rev. Lett.* **131** 030401
[16] Solanki P, Mehdi F M, Hajdušek M, and Vinjanampathy S 2023 *Phys. Rev. A* **108** 022216
[17] Cabot A, Giorgi G L, and Zambrini R 2021 *Proc. R. Soc. A.* **477** 20200850
[18] Lee T E, Chan C K, and Wang S 2014 *Phys. Rev. E* **89** 022913
[19] Walter S, Nunnenkamp A, and Bruder C 2014 *Phys. Rev. Lett.* **112** 094102
[20] Aifer M, Thingna J, and Deffner S 2024 *Phys. Rev. Lett.* **133** 020401
[21] Schmolke F and Lutz E 2022 *Phys. Rev. Lett.* **129** 250601
[22] Schmolke F and Lutz E 2024 *Phys. Rev. Lett.* **132** 010402
[23] Wächtler C W and Moore J E 2024 *Phys. Rev. Lett.* **132** 196601
[24] Laskar A. W, Adhikary P, Mondal S, Katiyar P, Vinjanampathy S, and Ghosh S 2020 *Phys. Rev. Lett.* **125** 013601
[25] Zhang L, Wang Z, Wang Y, Zhang J, Wu Z, Jie J, and Lu Y 2023 *Phys. Rev. Res.* **5** 033209
[26] Li Y, Xie Z, Yang X, Li Y, Zhao X, Cheng X, Peng X, Li J, Lutz E, Lin Y, and Du J 2025 *Sci. Adv.* **11** eady5649
[27] Krithika V R, Solanki P, Vinjanampathy S, and Mahesh T S 2022 *Phys. Rev. A* **105** 062206
[28] Koppenhöfer M, Bruder C, and Roulet A 2020 *Phys. Rev. Res.* **2** 023026
[29] Ying L, Lai Y C, and Grebogi C 2014 *Phys. Rev. A* **90** 053810
[30] Zhou K J, Zou J, and Shao B 2023 *Phys. Rev. A* **108** 042206
[31] Rau J 1963 *Phys. Rev.* **129** 1880
[32] Caves C M and Milburn G J 1987 *Phys. Rev. A* **36** 5543
[33] Scarani V, Ziman M, Štelmachovič P, Gisin N, and Bužek V 2002 *Phys. Rev. Lett.* **88** 097905
[34] Ziman M, Štelmachovič P, Bužek V, Hillery M, Scarani V, and Gisin N 2002 *Phys. Rev. A* **65** 042105
[35] Karevski D and Platini T 2009 *Phys. Rev. Lett.* **102** 207207
[36] Giovannetti V and Palma G M 2012 *Phys. Rev. Lett.* **108** 040401
[37] Ciccarello F, Palma G M, and Giovannetti V 2013 *Phys. Rev. A* **87** 040103
[38] Cattaneo M, De Chiara G, Maniscalco S, Zambrini R, and Giorgi G L 2021 *Phys. Rev. Lett.* **126** 130403
[39] Cattaneo M, Rossi M A C, García-Pérez G, Zambrini R, and Maniscalco S 2023 *PRX Quantum* **4** 010324
[40] Karpat G, Yalçinkaya İ, Çakmak B, Giorgi G L, and Zambrini R 2021 *Phys. Rev. A* **103** 062217
[41] Zhang Q, Man Z X, Zhang Y J, Yan W B, and Xia Y J 2023 *Phys. Rev. A* **107** 042202
[42] Breuer H P and Petruccione F 2007 *The Theory of Open Quantum Systems* (Oxford University Press)
[43] Jozsa R 1994 *J. Mod. Opt.* **41** 2315
[44] Van Kampen N G 1992 *Stochastic processes in physics and chemistry* (Elsevier, Amsterdam) **1**
[45] Wiseman H M and Milburn G J 2009 *Quantum Measurement and Control* (Cambridge University Press)
[46] Brown H R, Myrvold W, and Uffink J 2009 *Stud. Hist. Philos. Sci. B* **40** 174
[47] Ciccarello F, Lorenzo S, Giovannetti V, and Palma G M 2022 *Phys. Rep.* **954** 1
[48] Reiter F and Sørensen A S 2012 *Phys. Rev. A* **85** 032111
[49] Murch K W, Vool U, Zhou D, Weber S J, Girvin S M, and Siddiqi I 2012 *Phys. Rev. Lett.* **109** 183602
[50] Morigi G, Eschner J, Cormick C, Lin Y, Leibfried D, and Wineland D J 2015 *Phys. Rev. Lett.* **115** 200502
[51] Ma R, Saxberg B, Owens C, Leung N, Lu Y, Simon J, and Schuster D I 2019 *Nature* **566** 51
[52] Lin R, Rosa-Medina R, Ferri F, Finger F, Kroeger K, Donner T, Esslinger T, and Chitra R 2022 *Phys. Rev. Lett.* **128** 153601
[53] Rodrigues F L S, De Chiara G, Paternostro M, and Landi G T 2019 *Phys. Rev. Lett.* **123** 140601
[54] Karpat G, Yalçınkaya İ, and Çakmak B 2019 *Phys. Rev. A* **100** 012133
[55] Karpat G, Yalçınkaya İ, and Çakmak B 2020 *Phys. Rev. A* **101** 042121
[56] Mahlow F, Çakmak B, Karpat G, Yalçınkaya İ, and Fanchini F F 2024 *Phys. Rev. A* **109** 052411
[57] Wootters W K 1998 *Phys. Rev. Lett.* **80** 2245
[58] Nielsen M A 1999 *Phys. Rev. Lett.* **83** 436
[59] Es'haqi-Sani N, Manzano G, Zambrini R, and Fazio R 2020 *Phys. Rev. Res.* **2** 023101
[60] Li X, Li Y, and Jin J 2023 *Phys. Rev. A* **107** 032219
[61] Li W 2022 *Phys. Rev. A* **106** 023512
[62] Hatano N and Suzuki M 2005 *Finding Exponential Product Formulas of Higher Orders* p. 37
[63] Javadi-Abhari A, Treinish M, Krsulich K, Wood C J, Lishman J, Gacon J, Martiel S, Nation P D, Bishop L S, Cross A W, Johnson B R, and Gambetta J M 2024 arXiv:2405.08810 [quant-ph]

[64] Morvan A, Ramasesh V V, Blok M S, Kreikebaum J M, O'Brien K, Chen L, Mitchell B K, Naik R K, Santiago D I, and Siddiqi I 2021 *Phys. Rev. Lett.* **126** 210504
[65] Goss N, Morvan A, Marinelli B, Mitchell B K, Nguyen L B, Naik R K, Chen L, Jünger C, Kreikebaum J M, Santiago D I, Wallman J J, and Siddiqi I 2022 *Nat. Commun.* **13** 7481
[66] Luo K, Huang W, Tao Z, Zhang L, Zhou Y, Chu J, Liu W, Wang B, Cui J, Liu S, Yan F, Yung M H, Chen Y, Yan T, and Yu D 2023 *Phys. Rev. Lett.* **130** 030603
[67] Roy T, Li Z, Kapit E, and Schuster DavidI 2023 *Phys. Rev. Appl.* **19** 064024
[68] Harrington P M, Mueller E J, and Murch K W 2022 *Nat. Rev. Phys.* **4** 660